Journal of Nuclear Materials 389 (2009) 377–384

Contents lists available at ScienceDirect

Journal of Nuclear Materials

journal homepage: www.elsevier.com/locate/jnucmat

3D finite element and experimental study of the size requirements for measuring toughness on tempered martensitic steels

P. Mueller *, P. Spätig

Fusion Technology-Materials, CRPP-EPFL, Association EURATOM-Confédération Suisse, 5232 Villigen PSI, Switzerland

ARTICLE INFO

Article history:
Received 31 October 2008
Accepted 30 January 2009

ABSTRACT

The fracture properties of the tempered martensitic steel Eurofer97, which is among the main candidates for fusion power plant structural applications, were studied with two sizes of pre-cracked compact specimens (0.35T C(T) and 0.87T C(T)). The fracture toughness behavior was characterized within the temperature range −80 to −40 °C. The ductile-to-brittle transition reference temperature, as defined in the ASTM standard E1921, was around $T_0 \approx -75$ °C. At −60 °C, it was found that two sets of toughness data obtained with 0.35T and 0.87T C(T) specimens are not consistent with the size adjustments recommended in the ASTM standard. It was then shown that the underlying reason of this inconsistency is an inappropriate specimen size limit of the ASTM standard for this type of steel. From published fracture toughness data on the tempered martensitic steel F82H steel, similar results were also highlighted. 3D finite elements simulations of the compact specimens were performed to compare the stresses and deformations at the onset of fracture. A local approach model based on the attainment of a critical stress and a critical volume was used to study the constraint loss phenomenon. Within the framework of this model, the strong toughness increase by reducing the specimen size could be satisfactorily explained.

1. Introduction

Thermonuclear fusion power appears as a promising energy source for the future to fulfill the growing energy need of the world population. One of the greatest challenges in the realization of a nuclear fusion power plant is the development of new materials able to sustain the aggressive irradiation environment of a burning deuterium–tritium plasma. For the last three decades, international fusion materials programs in Europe, Japan and US have been highly focused on the development of the so-called reduced-activation tempered martensitic steels. These steels are among the main candidate materials for structural applications due to low irradiation-induced swelling, good mechanical and thermal properties, and reasonably fast radioactive decay [1]. While being attractive materials, the major degradation of their mechanical properties is reflected by irradiation embrittlement, which is characterized by an upward shift of the ductile-to-brittle transition temperature when irradiated at temperatures below 400 °C [2]. Above this temperature, non-hardening embrittlement could also occur. For example, there is some experimental evidence that helium, produced by transmutation, precipitates in the form of bubbles on the grain boundaries, weakens these boundaries and promotes intergranular fracture at helium concentrations higher than about 400–600 appm [3].

In order to safely manage the operation conditions of the first wall and blanket structure of the future fusion reactors, methods to assess the irradiation-induced temperature shifts of the toughness-temperature curve from a limited number of irradiated specimens are required. For the tempered martensitic steels, it was proposed to apply the master-curve methodology initially developed for the low-alloyed reactor pressure vessel steels [2]. This methodology relies on the concept of universal toughness-temperature curve shape of all 'ferritic' steels in the transition region [4,5]. The master-curve is indexed at a reference temperature T_0 at a specific toughness usually equal to 100 MPa $m^{1/2}$. T_0 is a material dependent parameter. Note that the master-curve shape and T_0 actually depend on various parameters, namely, specimen size, specimen geometry, loading rate, crack length (a) to specimen width (W) ratio. The master-curve usually refers to 25.4 mm thick specimens (1T specimen), having $a/W = 0.5$, and loaded statically. The main advantage of the methodology is its capability to determine the reference temperature T_0 with a limited number of specimens. The procedures to determine T_0 are specified in the ASTM E 1921-08 standard [6].

While some doubts were cast about the applicability of the master-curve to tempered martensitic steels [7], the master-curve approach was shown to yield a reasonable description of the toughness behavior in the transition region provided that specimen size effect on measured toughness are properly accounted for [8,9]. Indeed, it is well known that measured fracture toughness depends on a variety of parameters, including in particular

* Corresponding author. Tel.: +41 56 310 4418; fax: +41 56 310 4529.
E-mail addresses: pablo.mueller@psi.ch, pablomueller@gmail.com (P. Mueller).

0022-3115/$ - see front matter © 2009 Elsevier B.V. All rights reserved.
doi:10.1016/j.jnucmat.2009.01.311

specimen size and geometry [2]. Thus specimen size and geometry effects on measured toughness have to be well understood in order to transfer these measured values from one specimen size to another. This is of primary importance for the nuclear materials research community that is in most of the cases forced to test small specimens when studying fracture properties for irradiated specimens. Further, transferring laboratory fracture toughness test data to technological applications is an important issue for structural integrity assessments of real structures.

As a matter of fact, specimen size issues are addressed in the ASTM E1921-08 standard that specifies: (i) a maximum allowable measured toughness related to the uncracked ligament to ensure that constraint loss does not occur and (ii) a toughness crack front length adjustment based upon statistical considerations to trigger a crack initiator in the process zone at the crack tip [10]. Two recent studies were performed on reactor pressure vessel steels to re-assess the size limit for cleavage toughness as stated in the ASTM E1921 standard [11,12]. In both investigations, it was shown that the ASTM E1921 size limit is too lenient, resulting in early constraint loss that in turn leads to non-conservative estimates of T_0.

The goal of this paper is to re-evaluate the specimen size requirements to determine conservative estimates of T_0 for a high-chromium reduced-activation tempered martensitic steel. The approach is based on an evaluation of experimental fracture data obtained on two different sub-sized compact tension specimens in the transition region. In addition, 3D finite element simulations of the compact tension specimens supplement the evaluation of the experimental toughness data in order to model and predict the observed specimen effects on measured toughness.

2. Material

The alloy investigated in this work is the reduced-activation tempered martensitic steel Eurofer97. The Eurofer97 steel is a high-chromium reduced-activation tempered martensitic steel. This steel was developed within the long term program of the European Fusion Development Agreement and is the reference material for the future test blanket module of ITER [13]. It contains 8.90 wt% Cr, 0.12 wt% C, 0.46 wt% Mn, 1.07 wt% W, 0.2 wt% V, 0.15 wt% Ta, and Fe for the balance. The final heat-treatment consisted of a normalization at 980 °C for 0.5 h and of a tempering at 760 °C for 1.5 h. The steel was fully martensitic after quenching. The prior austenite grain size was about 10 (ASTM). Note that in order to obtain the reduced-activation behavior, several alloying elements commonly added to commercial martensitic stainless steels like Ni, Nb and Mo have been replaced by W, V, Ta, which under neutron irradiation produce shorter half-life radionuclides. A detailed description of the microstructure of the Eurofer97 can be found in [14]. The fracture specimens were machined from the 25 mm thick plate, heat E83697, produced by Böhler AG.

3. Master-curve approach

The American Society of Testing Materials has developed the standard ASTM E 1921 [6] to measure a ductile-to-brittle transition reference temperature, T_0, from a small number of data, obtained with specimens tested within a temperature window of $T_0 \pm 50$ °C. This approach is a standardization of the Master curve method proposed by Wallin [15]. This method was initially developed and works fairly well for fission reactor pressure vessel low alloy steels. T_0 is defined as the temperature where the median fracture toughness (K_{Jc}) of 1T thickness ($B = 25.4$ mm) specimens is 100 MPa $m^{1/2}$. The standard master-curve is based on a universal shape of the temperature-median toughness curve, a Weibull description of the scatter and a statistical size effect associated to the crack front length.

The universal median toughness temperature dependence for 1T specimens is described by the following equation:

$$K_{Jc\_med}(T) = A + (100\ \text{MPa}\ \text{m}^{1/2} - A)\exp(C(T - T_0)). \quad (1)$$

With $A = 30$ MPa $m^{1/2}$ and $C = 0.019$/°C. T_0 is the only material dependent parameter.

The standard provides a toughness size adjustment if specimen thicknesses different from 1T are used. This correction accounts for the statistical size effect and reads:

$$K_1 = K_{min} + (K_2 - K_{min})\left(\frac{B_2}{B_1}\right)^{1/4} \quad (2)$$

with $K_{min} = 20$ MPa $m^{1/2}$.

The standard assumes that the cumulative failure probability of a dataset at a given temperature follows Eq. (3) if $K_{Jc} < K_{Jc\_limit}$.

$$P(K_{Jc} < K) = 1 - \exp\left(-\left(\frac{K - K_{min}}{K_0 - K_{min}}\right)^4\right) \quad (3)$$

with $K_0 = (K_{Jc\_med} - K_{min})\ln(2)^{-1/4} + K_{min}$. This means that K_0 corresponds to a 63.2% cumulative failure probability and is the temperature dependent parameter in Eq. (3).

The toughness limit K_{Jc_limit} is given by Eq. (4), with $M = 30$, $b_0 = W - a_0$, being a_0 the initial crack length, E the Young modulus, ν the Poisson ratio and σ_{ys} the yield stress. Note that $b_0 \approx B$ when $a/W \approx 0.5$ and that K_{Jc_limit} depends on the specimen size [10].

In addition to the specimen crack front length adjustment of Eq. (2), the issue of constraint loss is addressed in the ASTM standard by defining a specimen measuring capacity with the equation:

$$K_{Jc\_limit} = \sqrt{\frac{Eb_0\sigma_{ys}}{M(1-\nu^2)}}. \quad (4)$$

The standard assumes that the measured K_{Jc} values that fall below the K_{Jc_limit} are not affected by loss of constraint and that the distribution of these values will follow Eq. (3) for $K_{Jc} < K_{Jc\_limit}$. On the other end, for values greater than the limit, $K_{Jc} > K_{Jc\_limit}$, it is assumed that loss of constraint could have affected the measured K_{Jc} by increasing its apparent toughness and thus these values would not follow the mentioned distribution. Nonetheless, a value above the limit still carries some useful information: the toughness of the specimen was at least equal or greater than the limit because, before reaching the limit, it did not loose constraint and did not break. The standard combines these assumptions with Eqs. (1)–(4) in order to determine T_0 by means of the maximum likelihood method. This leads to Eq. (5) where T_0 can be determined by iteration.

$$\sum_{i=1}^{N}\delta_i\frac{\exp(0.019(T_i - T_0))}{11 + 77\exp(0.019(T_i - T_0))} - \sum_{i=1}^{N}\frac{(K_{Jc(i)} - 20)^4\exp(0.019(T_i - T_0))}{(11 + 77\exp(0.019(T_i - T_0)))^5} \quad (5)$$

with the temperatures in °C, K_J in MPa $m^{1/2}$ and: N = number of specimens tested; T_i = test temperature corresponding to $K_{Jc(i)}$; $K_{Jc(i)}$= either K_{Jc} (if $K_{Jc} < K_{Jc\_limit}$) or K_{Jc_limit} (if $K_{Jc} > K_{Jc\_limit}$); δ_i = either 1.0 (if $K_{Jc} < K_{Jc\_limit}$) or zero (if $K_{Jc} > K_{Jc\_limit}$).

4. Experimental procedures

4.1. Fracture tests

The experimental procedure used to measure fracture toughness was based on the ASTM E 1820 [16] standard. Standard

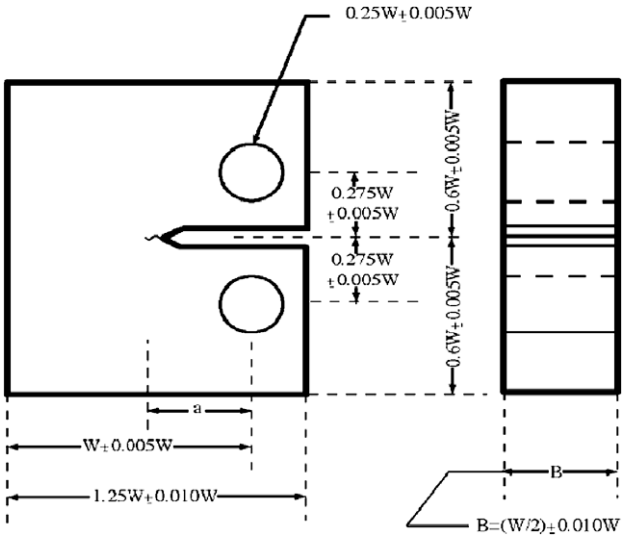

Fig. 1. Standard C(T) specimen.

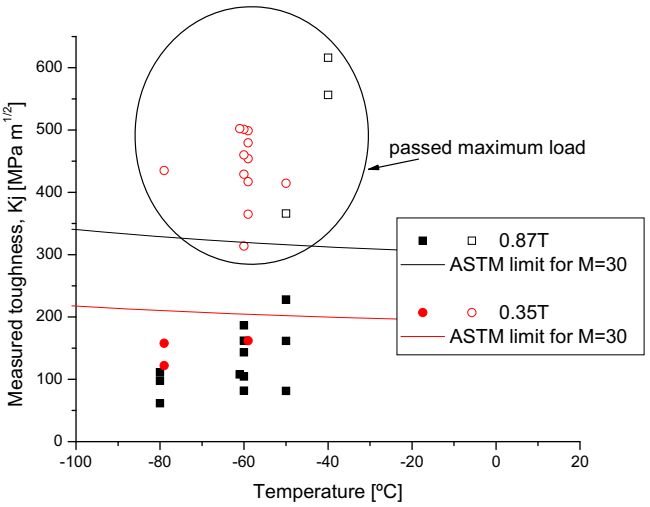

Fig. 3. Experimental Eurofer'97 steel fracture toughness data measured with C(T) specimens.

compact specimens (Fig. 1) tested in tension, called C(T) specimens, were produced in two sizes, namely 0.87T (B = 22 mm) and 0.35T (B = 9 mm). The specimens were cut in the L–T orientation. A provision to insert a clip gage in the front face of the specimen was machined on the 0.35T specimens (Fig. 7) to accurately measure the crack mouth opening displacement during the test. This allows a direct comparison with the finite elements simulations. The pre-cracks were introduced by fatigue at room temperature. The temperature of the specimens during the test was monitored with an attached thermocouple. The standard nine points crack length measurement was performed in order to determine the initial crack length ratio a/W. The average crack length ratio of the specimens was about a/W = 0.52. The stress intensity factor K_J was calculated in the standard way,

$$K_J = \sqrt{\frac{(J_e + J_{pl})E}{1-\nu^2}}. \quad (6)$$

In Fig. 4 the load–displacement curves measured with the clip gage are plotted for 0.35T specimens tested at −60 °C. The difference in load from specimen to specimen is attributed to small variation in the crack length ratio (a/W) and in the crack angle. The curve corresponding to specimen P5.2 represents an average load–displacement curve. Hence, this curve was used for comparison with that calculated from the finite element simulations, where the modeled crack length to specimen width ratio was a/W = 0.52.

4.2. Tensile tests

Tensile tests were carried out at −60 °C in order to obtain the plastic flow constitutive properties. DIN round specimens were used with 2.4 mm diameter and 13.2 mm gauge length. The displacement of the specimen was measured with an attached clip gage. The corresponding true stress versus true plastic strain curve is used as input for the finite element simulations presented in the following. The tests were performed at two strain rates, 3 tests at 10^{-4} 1/s, and 2 tests at 10^{-3} 1/s. Similar results were obtained from the five tests due to the low strain rate dependence at this temperature. The average 0.2% yield stress for each strain rate was 594 and 614 MPa respectively. The true stress versus true plastic strain curves obtained form each experiment along with the values used for the simulations are plotted in Fig. 2. Note that the strain hardening beyond necking was considered constant; this means that

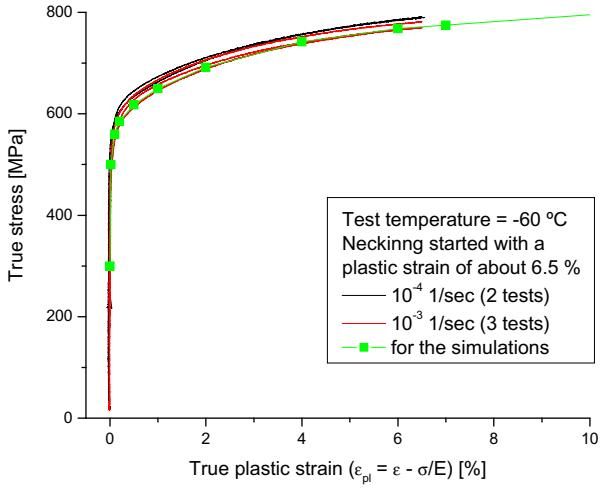

Fig. 2. Plastic flow curve of Eurofer97 steel at −60 °C.

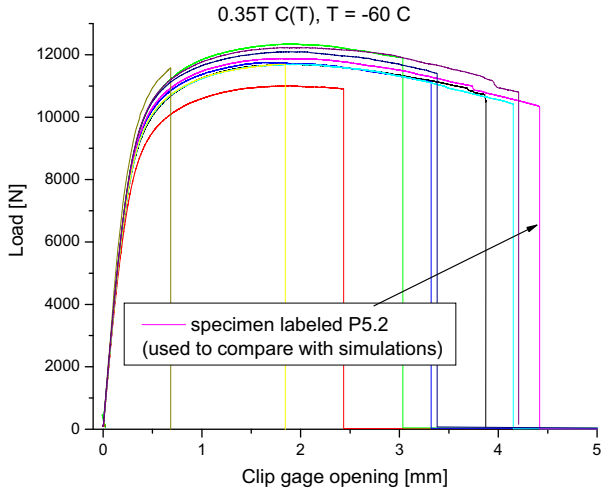

Fig. 4. Load–displacement curves of the specimens measured with an attached clip gage.

the plastic flow curve was linearly extrapolated beyond about 6.5% plastic true strain. This procedure was previously validated with the numerical reconstruction of the load–displacement curves of punch tests [17] and notched tensile specimens [18] for instance. In any case it was observed that for C(T) specimens the plastic properties beyond necking do not affect significantly the calculated stress fields and not at all the load–displacement curves.

5. Experimental results

5.1. Specimen size effect on measured fracture toughness

The fracture toughness data of Eurofer97 steel are shown in Fig. 3 along with the ASTM E1921 toughness limit (K_{Jc_limit}) for the two tested specimen sizes. The open symbols correspond to specimens having a load–deflection curve showing a load maximum. We recall that, within the framework of the ASTM E1921, this toughness limit is associated with an M value equal to 30. At −60 °C, K_{Jc_limit} of the 0.35T specimens is approximately 205 MPa $m^{1/2}$. For this temperature the median toughness of the six 0.87T C(T) specimens tested was 131 MPa $m^{1/2}$. Using the ASTM size adjustment, Eq. (2), the median toughness of the 0.87T C(T) specimens increases up to 159 MPa $m^{1/2}$ for the 0.35T C(T). Thus, 0.35T C(T) median toughness value is well below the K_{Jc_limit} calculated with $M = 30$. Consequently, we would expect to find about one half of the 0.35T values below 159 MPa $m^{1/2}$. However, from the eleven 0.35T specimens tested at −60 °C, ten broke between 300 and 500 MPa $m^{1/2}$ and only one at 162 MPa $m^{1/2}$. Clearly loss of constraint starts much before what is predicted by the toughness limit related to $M = 30$. This limit is not restrictive enough.

In addition, the minimum toughness value from the six 0.87T specimens measured at −60 °C was 82 MPa $m^{1/2}$. Using Eq. (2), this value corresponds to 97 MPa $m^{1/2}$ for a 0.35T specimen. Since none of the eleven 0.35T specimens tested at −60 °C was close to 97 MPa $m^{1/2}$, in fact all the values fell above 162 MPa $m^{1/2}$, it is clear that loss of constraint already occurs at such low deformation. An M limit value of about $M = 134$ is needed to have a K_{Jc_limit} = 97 MPa $m^{1/2}$ for 0.35T specimens.

We also found similar results when analyzing Sokolov and Tanigawa [19,20] C(T) fracture data of F82H steel. F82H is a reduced-activation tempered martensitic steel like Eurofer97 but with less Chromium. Both of these steels have practically the same elastic properties and similar yield stress. While only one of the five 1T specimens tested at −50 °C and reported in Table 1 showed a high toughness value, seven out of the eight 0.4T specimens presented very high values of toughness. Among the big specimens (1T), 4 out of 5 have broken below 150 MPa $m^{1/2}$. Using Eq. (2) this value corresponds to 183 MPa $m^{1/2}$ for a 0.4T specimen. Since the toughness limit related to $M = 30$ for a 0.4T size specimen is K_{Jc_limit} = 219 MPa $m^{1/2}$, we would expect to find most of the 0.4T specimens below 183 MPa $m^{1/2}$. Only 1 over 8 of the small specimens (0.4T) broke below 300 MPa $m^{1/2}$. Again the experimental results show clearly that loss of constraint started much before the standard ASTM limit, which means that a toughness limit related to $M = 30$ is not restrictive enough.

Table 1
F82H C(T) specimens tested at −50 °C by Sokolov et al.

Size	Measured toughness (MPa $m^{1/2}$)
1T	94.6
1T	114.6
1T	128.4
1T	146.7
1T	412.4
0.4T	124.5
0.4T	306.0
0.4T	322.9
0.4T	335.9
0.4T	340.6
0.4T	359.1
0.4T	393.0
0.4T	394.4

5.2. T_0 dependence with M limit

In order to better evaluate the K_{Jc_limit}, and find an M limit which is really representative of the onset of the measurable constraint loss influence on toughness, multi-temperature T_0 determinations (Eq. (5)) were performed for the Eurofer97 fracture data plotted in Fig. 3. Fig. 5 shows T_0 as a function of the M limit value. Clearly T_0 is still significantly dependent on M for values around $M = 30$, where a strong T_0 increase is observed with M. For M greater than about 135, T_0 oscillates around $T_0 \approx -75$ °C which is in good agreement with $T_0 = -78$ °C that we reported in [9]. The standard requires a minimum of six valid data points, namely points lying below K_{Jc_limit}. For $M > 270$ this criterion is not fulfilled (Fig. 6), which explains the increase in the amplitude of the T_0 oscillations. In

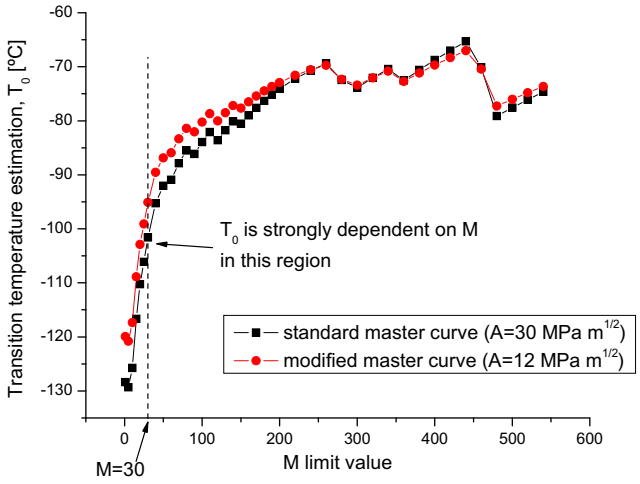

Fig. 5. Transition temperature (T_0) determination using the data tested at temperatures above −90 °C. T_0 is strongly dependent on the M value in the $M < 100$ region. A maximum toughness limit related to $M = 30$ is not appropriate for this material.

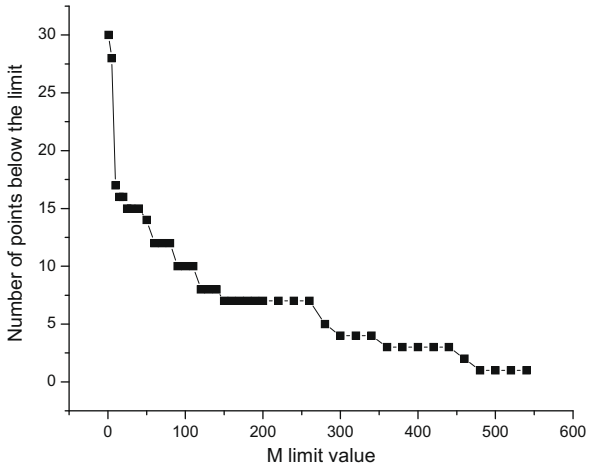

Fig. 6. Number of points below the maximum toughness limit in function of M. The standard requires a minimum of 6 valid data points. For $M > 270$ the number of valid points is too low.

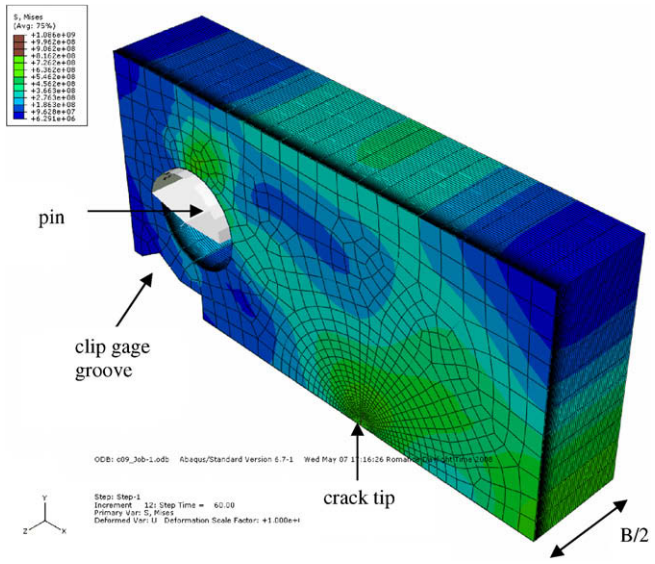

Fig. 7. Finite element model of the C(T) specimen. The loading pin and the clip gage notch are included in the model.

[9], the A value of Eq. (1) was fitted with the method of the maximum likelihood according to [21,22] in order to adjust the athermal part of the master-curve to the data tested at low temperature ($T < -100$ °C). The effect of this adjustment is not important at higher temperatures. This is also reflected in Fig. 5.

6. Finite element simulations

In order to study the loss of constraint that is responsible for the strong size effect observed in the experiments, three dimensional finite element simulations of the C(T) specimens tested at −60 °C were performed. The code used for the simulations was ABAQUS/Standard 6.7. Symmetric boundary conditions allow solving only one quarter of the specimen reducing the number of elements of the model by a factor four. 8-node linear brick elements have been used. Plastic deformation was included in the model, the material properties were considered isotropic, the Young modulus was $E = 212.5$ GPa, the Poisson ratio $\nu = 0.33$ and the plastic flow curve corresponds to that plotted in Fig. 2 and described in Section 4.2. A general view of the specimen along with the mesh is depicted in Fig. 7. The specimen was loaded by imposing the displacement to a frictionless rigid body pin, with the same diameter of the pin used in the experiments. The provision for the clip gage in the specimen front face machined in the 0.35T specimens was also included in the numerical model. This allows comparing at the same position the displacement measured experimentally by the clip gage with that obtained from the numerical simulations. The 0.87T C(T) specimens and the 0.35T C(T) ones had both an average crack length of approximately $a/W = 0.52$. This value of a/W was used for the simulations.

A finite initial crack tip radius (ρ_0) was used in the simulations, see Fig. 8. The effect of ρ_0 was studied using five models with different ρ_0/W ratios, namely $9000\rho_0/W = 1$, 2, 4, 8 and 16. The load–displacement curve was found to be independent of ρ_0 in the studied range. On the one hand, a large value of ρ_0 allows reaching large displacements of the pin without producing too severe deformation of the elements on the crack tip. On the other hand, for small loads, small values of ρ_0 are needed to have a good description of the stress fields close to the crack tip. This is shown and explained in detail in the following sections.

6.1. Load–displacement curves

In Fig. 9 we compare the experimental and simulated load–displacement curves for the 0.35T size specimens. As mentioned above, the displacement of these specimens was measured with a clip gage. The specimen chosen for the comparison was one with an average load–displacement curve (see Fig. 4). As shown in Fig. 9, there is very good agreement between the calculated curve and the experimental one for openings below 1 mm. Fractographic observations of the broken specimens showed that a small amount of ductile tearing occurred for specimens that passed maximum load. At openings larger than 1 mm, ductile tearing starts on the real specimen, the crack starts to grow in a stable manner and the load reaches a maximum, decreasing afterwards. This stable crack growth was not modeled. In this work, only the simulations of specimens breaking before maximum load were considered. They reproduce the loading of a specimen with a stable blunting crack under increasing load. Thus, the stress fields analyzed in this work correspond to those of the specimens representative of the lower part of toughness distribution (below maximum load). We can also see in Fig. 9 that there is no appreciable effect of ρ_0 on the load–displacement curve.

For the 0.87T C(T) specimens the displacement of the load train was measured. The pin displacement was obtained by performing the compliance correction of the machine. Fig. 10 compares the 0.87T simulations and experiments. Again we find very good agreement between them. An experiment performed at a temperature of 10 °C higher is also included in the figure. This specimen broke after more deformation giving an idea of the load–displacement curve we would get with a tough specimen at −60 °C. The breaking points of the experiments can also be seen in the figure.

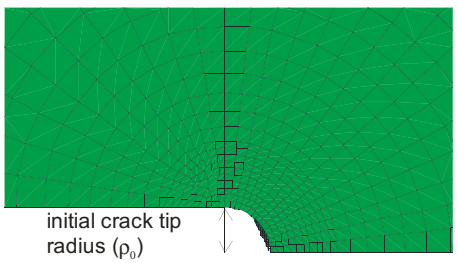

Fig. 8. View of the mesh close to the crack tip.

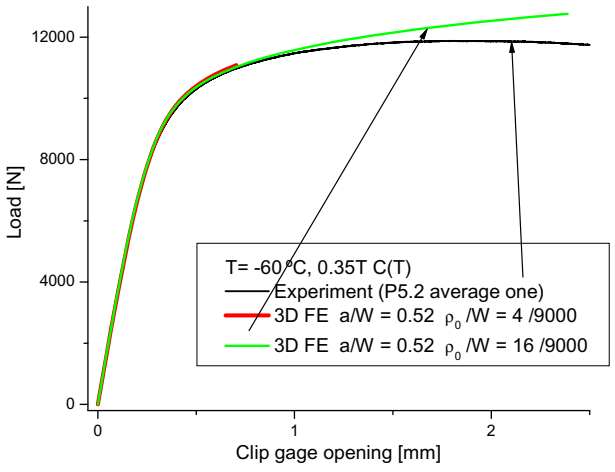

Fig. 9. Experimental and numerical load–displacement curves.

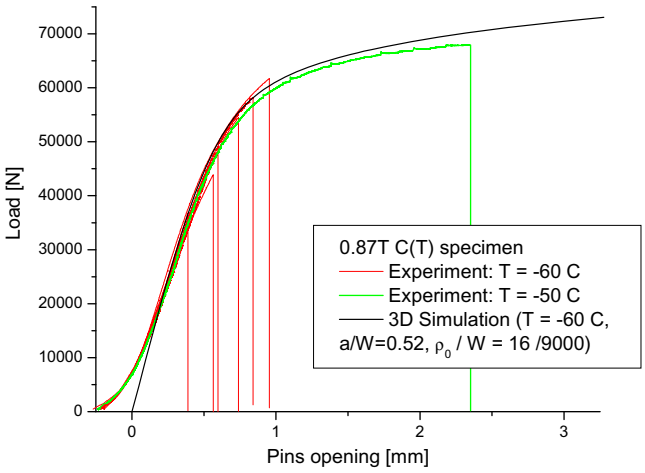

Fig. 10. Experimental and numerical load–displacement curves for the 0.87T specimens.

Experimentally the stress intensity factor K_J was calculated using the ASTM standard procedure [16]. Since the simulated curves were shown to reconstruct very well the experimental ones, the calculated K_J values reported in this work were obtained from the simulated curves by using the same equations as those in ASTM standard to determine the experimental K_J. However, it was verified that these last K_J values are consistent with the K_J values obtained from the calculated specimen thickness average J-integral.

6.2. Local approach: σ^*–V^* model

By means of finite element simulations the stresses and strains can be calculated in a cracked specimen or structure. The aim of a local approach model is to predict the critical stress/strain fields around a stress concentrator, crack or notch, which mediate the unstable propagation of a crack through the specimen. The pioneering work in the local approach was done by Ritchie et al. [23] who showed that the toughness temperature dependence of mild steel can be modeled with a critical condition defined by the attainment of a critical stress σ^* over critical distance ahead λ^* of the crack tip. Later, Wallin [24] calculated the statistical effects in toughness results based on the probability of encountering a particle having a radius satisfying the modified Griffith's criterion within the plastic zone around the crack tip. Thus, a direct link between the critical stress, the particle size and the particle size distribution and density was established. In addition, the failure probability was shown to follow a Weibull distribution with the applied stress intensity factor K as variable. Beremin [25] also developed a local model to deal with the statistical effects, based on the probability of finding a critical micro-crack in the plastic zone. In Beremin's model the cumulative failure probability is expressed with a two parameter Weibull distribution, the variable being the so-called Weibull stress that depends on the applied stress intensity factor. Gao et al. [26] proposed a sophisticated calibration procedure to determine the two parameters in Beremin's equation, which requires the use of fracture data obtained with high and low constraint specimen configurations as well as detailed 3D finite element simulations (such experimental data are not available in this work). The σ^*–V^* model [27], which represents the attainment of equivalent stressed volume V^* for a given critical stress σ^*, is another approach mainly used as a 'toughness-scaling' model to predict the toughness variation from one specimen size to another. In its simple form, the statistical effects are not taken into account. In this study, we focused on the constraint loss effect and toughness scaling between two different specimen sizes, so we made use of the σ^*–V^* model.

The stressed volume V^* is defined as the volume of material where the maximum principal stress, σ_1, is greater than σ^* ($\sigma_1 > \sigma^*$). For a given specimen geometry, material properties (constitutive equation) and temperature, V^* is function of σ^* and the applied stress intensity factor K_J.

$$V^* = f(\sigma^*, K_J). \tag{7}$$

In Fig. 11 we show the stressed volume V^* for $\sigma^* = 1500$ MPa. V^* was calculated from five models with different initial crack tip radius ρ_0. We see that after a short transient, V^* becomes practically independent of ρ_0. This transient decreases when ρ_0 is decreased converging to the case of an initial sharp crack tip when $\rho_0 \to 0$. In Fig. 12 we see the same plot as before but with $\sigma^* = 1900$ MPa. For higher values of σ^*, the effect of ρ_0 lasts longer, in terms of loading, because the volume of material under high stress is confined closer to the crack tip, where the influence of ρ_0 is more pronounced.

For the application of the fracture model explained below, we considered only the segments of the $V^*(K_J)$ curve that appeared to be independent of ρ_0. The stressed volume V^* as a function of K_J was piecewise fitted for each value of σ^* used in this work.

The σ^*–V^* local approach model is based on the following assumption: Brittle fracture of the specimen will occur with a certain probability when V^*, related to $\sigma^* = \sigma_c^*$, reaches a critical value called V_c^*. For this model the material properties are the critical parameters, σ_c^* and V_c^*. These parameters are usually considered temperature independent in the transition range. This brittle fracture local approach model has been used to estimate the ductile-to-brittle transition temperature in tempered martensitic steels [28], to model irradiation embrittlement [2] and constraint loss size effects in pressure vessel ferritic steels [29], to predict the temperature dependence of the lower bound of C(T) specimens [30] and of notched tensile specimens [18] for Eurofer97, among other works.

We recall first that for plane strain and small scale yielding (SSY) conditions the stressed area, A^*, has the following well known dependence on K_J:

$$A^* = cK_J^4, \tag{8}$$

where c is a constant that depends on σ^* and constitutive properties. This equation is also the limit solution close to the crack tip for a specimen with a sharp crack under a low applied K_J, i.e. when the plastic zone size is much smaller than the characteristic

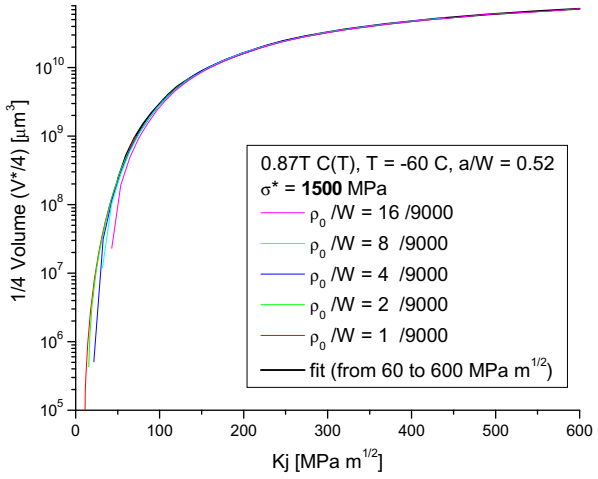

Fig. 11. Volume of the specimen where the maximum principal stress is higher than 1500 MPa in function of the applied K_J.

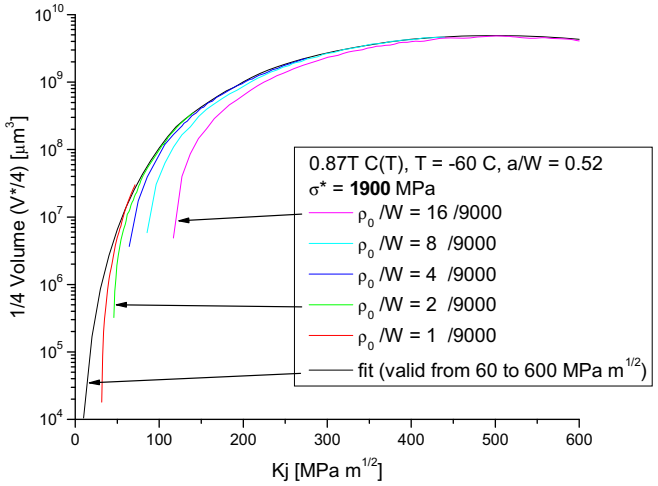

Fig. 12. Volume of the specimen where the maximum principal stress is higher than 1900 MPa in function of the applied K_J.

specimen dimensions, ligament and crack front length. If we apply the σ^*–V^* model to the SSY case with a specimen of thickness B then:

$$V^* = BA^* = BcK_J^4. \tag{9}$$

If a specimen of thickness B_1 breaks with a stress intensity factor K_{J1} then a specimen of thickness B_2 will reach the same critical volume for K_{J2}:

$$V^* = B_1 cK_{J1}^4 = B_2 cK_{J2}^4. \tag{10}$$

This gives a size effect of the form:

$$\frac{K_{J2}}{K_{J1}} = \left(\frac{B_1}{B_2}\right)^{1/4} \tag{11}$$

which is similar to the ASTM size adjustment Eq. (2) but without the minimum toughness K_{min}.

For large values of K_J, the SSY description of the stress fields does not hold anymore. In this case, the stress field close to the crack tip is influenced by the boundaries of the specimen so that it is not any more mediated by K_J only but also by the crack front length and ligament length. If two different specimen sizes/geometries are considered, referred as to #1 and #2 hereafter, V^* associated with each specimen remains given by Eq. (7) but two different functions f characterize the K_J and σ^* dependence on V^*:

$$\begin{aligned} V_1^* &= f_1(K_{J,1}, \sigma^*) \text{ specimen } \#1 \\ V_2^* &= f_2(K_{J,2}, \sigma^*) \text{ specimen } \#2 \end{aligned} \tag{12}$$

f_1 and f_2 are two functions that can be used to rescale fracture toughness data from one specimen size to another on the basis of the σ^*–V^* model. Indeed, Eq. (12) can be inverted to express K_J as a function of the other two variables for each specimen size as:

$$\begin{aligned} K_{J,1} &= h_1(V_1^*, \sigma^*) \text{ specimen } \#1 \\ K_{J,2} &= h_2(V_2^*, \sigma^*) \text{ specimen } \#2 \end{aligned}. \tag{13}$$

By making $V_1^* = V_2^* = V^*$, the scaling law between the two specimens then reads:

$$K_{J,2} = h_2(V^*, \sigma^*) = h_2(f_1(K_{J,1}, \sigma^*), \sigma^*). \tag{14}$$

In order to quantify this phenomenon of constraint loss, we rely on 3D numerical simulations to calculate the f_i functions. In Fig. 13 the stressed volume is plotted for σ^* = 1955 MPa. Note that this value was recently shown to be the critical stress that allows reconstructing the temperature dependence of the 1% failure probability curve of the master-curve [30]. As can be seen, the stressed volume

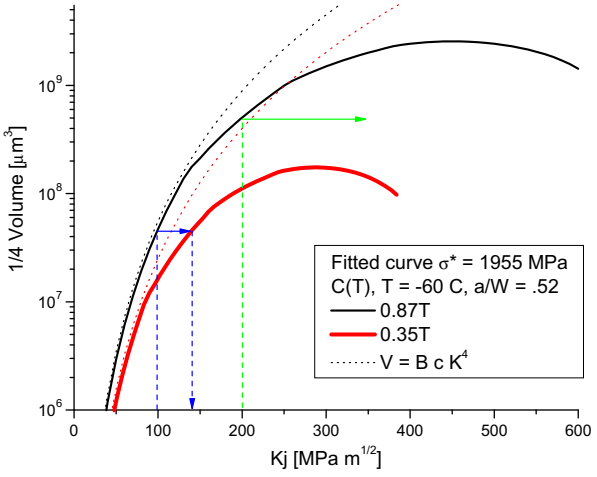

Fig. 13. Model application example. A 0.87T size specimen that breaks at 100 MPa $m^{1/2}$ corresponds to a 0.35T specimen breaking at 140 MPa $m^{1/2}$. For a 0.87T specimen loaded to 200 MPa $m^{1/2}$ this critical condition cannot be reached by a 0.35T specimen, indicating that a large toughness increase is expected.

in a 0.35T C(T) specimen does not follow Eq. (9) for K_J higher than about 80 MPa $m^{1/2}$. This means that for a 0.87T C(T) specimen with K_J higher than about 60 MPa $m^{1/2}$ the model predicts a higher toughness increase to 0.35T than Eq. (11). In Fig. 13 we also see that V^* reaches a maximum. Because of this maximum it is impossible to reach with a 0.35T C(T) specimen the stressed volume that a 0.87T C(T) specimen has when K_J is higher than about 140 MPa $m^{1/2}$. This indicates that a strong toughness increase can be expected and possibly also a change in the fracture mechanism.

A parametric study of the model is shown in Fig. 14 to illustrate the effect of the critical stress on the toughness scaling from 0.87T to 0.35T C(T) specimens. The expected toughness increase ΔK_J from the 0.87T to 0.35T C(T) specimens is calculated using Eq. (14) that can be readily rewritten as:

$$\Delta K_J = K_{0.35T} - K_{0.87T} = h_2(f_1(K_{0.87T}, \sigma^*), \sigma^*) - K_{0.87T}. \tag{15}$$

Using Eq. (15), we calculated the toughness increase to 0.35T predicted by the model for the six 0.87T experimental values obtained, and we compare them with the ASTM Eq. (2) prediction. Clearly the strong loss of constraint effect observed with the σ^*–V^* model is reflected by the experiments. We recall again that that this toughness model scaling is not intended to describe the probabilistic nature of cleavage.

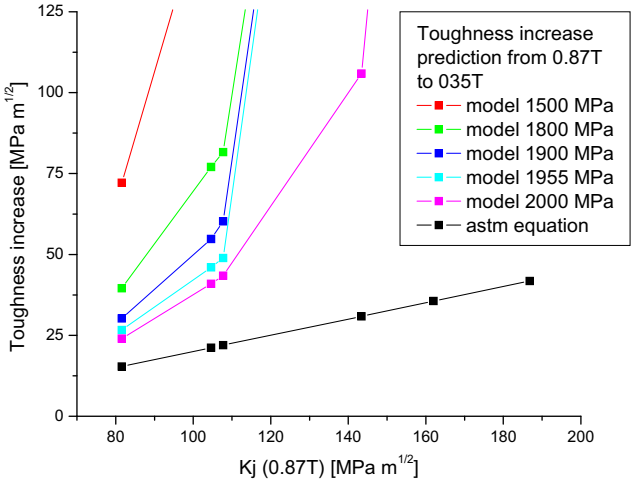

Fig. 14. 0.35T to 0.87T toughness increase prediction of the σ^*–V^* model for different critical parameters along with the standard prediction.

7. Conclusions

In this work we studied the fracture size effect of the reduced-activation tempered martensitic steel Eurofer97 mainly in the temperature range −80 to −40 °C. Two sizes of pre-cracked specimens were tested, namely 0.87T and 0.35T. 3D finite element simulations of the specimens were performed in order to study the predictions of a local approach type model called σ^*–V^*.

- Even when the ASTM size requirements associated with $M = 30$ were fulfilled, the 0.35T C(T) specimens yielded a 1T-adjusted toughness value much higher than the expected values. This clearly indicates that the $M = 30$ limit is too lenient for the tempered martensitic steels. In order to avoid this problem a value greater than about 135 is required.
- Similar results were found on F82H, another tempered martensitic steel with less chromium than Eurofer97.
- Another clear indication that $M = 30$ is too low for this material is the fact that the ductile-to-brittle transition temperature, T_0, has a significant dependence with M for values below 135.
- It was shown that the 3D finite element simulations reproduced very well the load–displacement curves of the specimens up to the initiation of stable crack growth. No appreciable effect of the initial crack tip radius on the load–displacement curve was observed for the studied values, $\rho_0/W < 16/9000$.
- The constraint loss effects on measured toughness were quantified using a critical condition for fast-fracture based on the attainment of a critical stress σ^* within a critical volume V^*. It was shown that special attention has to be paid to the effect of the initial crack tip radius, ρ_0 on V^*. Indeed, for values of σ^* close to the peak stress value, and for small crack tip opening, V^* depends on ρ_0. For low values of σ^*, V^* gets quickly independent of ρ_0 by increasing the applied K, even if the crack tip of the model is not blunted.
- The size effect predictions based on the σ^*–V^* model were found consistent with a strong size effect observed in the experiments. The size effect was found much larger than the B-adjustment recommended in the ASTM E1921.

Acknowledgements

The financial support of the Swiss National Foundation is gratefully acknowledged. This work, supported by the European Communities under the contract of Association between EURATOM/Switzerland, was carried out within the framework of the European Fusion Development Agreement (EFDA). The views and opinions expressed herein do not necessarily reflect those of the European Commission. The Paul Scherrer Institute is acknowledged for providing access to its facilities.

References

[1] R.L. Klueh, Curr. Opin. Solid State Mater. Sci. 8 (2004) 239.
[2] G.R. Odette, T. Yamamoto, H.J. Rathbun, M.Y. He, M.L. Hribernik, J.W. Rensman, J. Nucl. Mater. 323 (2003) 313.
[3] T. Yamamoto, G.R. Odette, H. Kishimoto, J.W. Rensman, P. Miao, J. Nucl. Mater. 356 (2006) 27.
[4] K. Wallin, ASME PVP 170 (1989) 93.
[5] K. Wallin, Int. J. Pres. Ves. Piping 55 (1993) 61.
[6] ASTM, E 1921 - 08, in: Standard Test Method for Determination of Reference Temperature, T_0, for Ferritic Steels in the Transition Range, 2008.
[7] E. Lucon, J. Nucl. Mater. 367–370 (2007) 575.
[8] G.R. Odette, T. Yamamoto, H. Kishimoto, M. Sokolov, P. Spätig, W.J. Yang, J.W. Rensman, G.E. Lucas, J. Nucl. Mater. 329–333 (2004) 1243.
[9] P. Mueller, P. Spätig, R. Bonadé, G.R. Odette, D. Gragg, J. Nucl. Mater. (2008), doi:10.1016/j.jnucmat.2008.12.122.
[10] K. Wallin, J. Phys. IV (Suppl. J. Phys. III 3, Colloque C7) (1993) 575.
[11] J.A. Joyce, R.L. Tregoning, Engng. Fract. Mech. 72 (2005) 1559.
[12] H.J. Rathbun, G.R. Odette, M.Y. He, T. Yamamoto, Engng. Fract. Mech. 73 (2006) 2723.
[13] N. Baluc, D.S. Gelles, S. Jitsukawa, A. Kimura, R.L. Klueh, G.R. Odette, B. v. d. Schaaf, J. Yu, J. Nucl. Mater. 367–370 (2007) 33.
[14] P. Fernández, A.M. Lancha, J. Lapeña, M. Hernández-Mayoral, Fus. Eng. Des. 58&59 (2001) 787.
[15] K. Wallin, Int. J. Mater. Prod. Technol. 14 (1999) 342.
[16] ASTM, E 1820 - 08, in: Standard Test Method for Measurement of Fracture Toughness, 2001.
[17] E.N. Campitelli, P. Spätig, R. Bonadé, W. Hoffelner, M. Victoria, J. Nucl. Mater. 335 (2004) 366.
[18] P. Mueller, R. Bonadé, P. Spätig, Mater. Sci. Eng. A 483&484 (2008) 346.
[19] M.A. Sokolov, H. Tanigawa, J. Nucl. Mater. 367–370 (2007) 587.
[20] M.A. Sokolov, H. Tanigawa, in: Fusion Materials Semiannual Progress Report for the period ending December 31, 2006, DOE-ER-0313/41, p. 85.
[21] K. Wallin, in: Recent Advances in Fracture (Proceedings of the International Conference Orlando, 1997) Minerals, Metals, and Materials Society, Warrendale, PA, 1997, p 171.
[22] IAEA, in: Technical reports series No. 429, "Guidelines for application of the master curve approach to a reactor pressure vessel integrity in nuclear power plants", IAEA, Vienna, 2005.
[23] R.O. Ritchie, J.F. Knott, J.R. Rice, J. Mech. Phys. Solids 21 (1973).
[24] K. Wallin, Engng. Fract. Mech. 19 (1984) 1085.
[25] F.M. Beremin, Metall. Trans. A 14A (1983) 2277.
[26] X. Gao, C. Ruggieri, R.H. Dodds, Int. J. Fract. 92 (1998) 175.
[27] R.H. Dodds, C.F. Shih, T.L. Anderson, Int. J. Fract. 64 (1993) 101.
[28] G.R. Odette, J. Nucl. Mater. 212–215 (1994) 45.
[29] H.J. Rathbun, G.R. Odette, M.Y. He, T. Yamamoto, Engng. Fract. Mech. 73 (2006) 2723.
[30] R. Bonadé, P. Mueller, P. Spätig, Engng. Fract. Mech. 75 (2008) 3985.